

Transmission of 273.6 Tb/s Over 1001 km of 15-Mode Multi-Mode Fiber Using C-Band Only 16-QAM Signals

Menno van den Hout ¹, *Student Member, IEEE, Optica*, Giammarco Di Sciullo ², *Student Member, IEEE*, Ruben S. Luís ³, *Senior Member, IEEE*, Benjamin J. Puttnam ³, *Member, IEEE*, Nicolas K. Fontaine ⁴, *Fellow, IEEE, Optica*, Roland Ryf ⁵, *Fellow, IEEE, Optica*, Haoshuo Chen ⁶, Mikael Mazur ⁷, *Member, IEEE*, David T. Neilson ⁸, *Fellow, IEEE*, Pierre Sillard ⁹, Frank Achten, Ali Mefleh ¹⁰, Jun Sakaguchi ¹¹, *Member, IEEE*, Cristian Antonelli ¹², *Senior Member, IEEE, Fellow, Optica*, Chigo Okonkwo ¹³, *Senior Member, IEEE*, Hideaki Furukawa, *Member, IEEE*, and Georg Rademacher ¹⁴, *Senior Member, IEEE*

(Post-Deadline Paper)

Abstract—In recent years, space-division multiplexing (SDM) has been proposed and investigated as a technique to increase the per-fiber capacity in order to cope with the ever-increasing demand for capacity in optical transmission networks. Considering the various SDM architectures proposed, multi-mode fibers potentially allow for the highest spatial channel density, but

Manuscript received 30 June 2023; revised 17 August 2023 and 13 September 2023; accepted 15 September 2023. Date of publication 19 September 2023; date of current version 2 February 2024. This work was supported in part by the TU/e-KPN flagship Smart Two project, and in part by the PhotonDelta Dutch National Growth Funds for Photonics and the Italian Government through Projects INCIPICT and FIRST. (Corresponding author: Menno van den Hout.)

Menno van den Hout is with the Photonic Network System Laboratory, National Institute of Information and Communications Technology, Tokyo 184-8795, Japan, and also with the High Capacity Optical Transmission Laboratory, Electro-Optical Communications Group, Eindhoven University of Technology, 5600 MB Eindhoven, The Netherlands (e-mail: m.v.d.hout@tue.nl).

Giammarco Di Sciullo is with the Photonic Network System Laboratory, National Institute of Information and Communications Technology, Tokyo 184-8795, Japan, and also with the University of L'Aquila and CNIT, 67100 L'Aquila, Italy (e-mail: giammarco.disciullo@graduate.univaq.it).

Ruben S. Luís, Benjamin J. Puttnam, Jun Sakaguchi, and Hideaki Furukawa are with the Photonic Network System Laboratory, National Institute of Information and Communications Technology, Tokyo 184-8795, Japan (e-mail: rluis@nict.go.jp; ben@nict.go.jp; jsakaguchi@nict.go.jp; furukawa@nict.go.jp).

Nicolas K. Fontaine, Roland Ryf, Haoshuo Chen, Mikael Mazur, and David T. Neilson are with the Nokia Bell Labs, New Providence, NJ 07974 USA (e-mail: nicolas.fontaine@nokia-bell-labs.com; roland.ryf@nokia-bell-labs.com; haoshuo.chen@nokia-bell-labs.com; mikael.mazur@nokia-bell-labs.com; david.neilson@nokia-bell-labs.com).

Pierre Sillard is with the Prysmian Group, 62092 Haisnes Cedex, France (e-mail: pierre.sillard@prysmiangroup.com).

Frank Achten is with the Prysmian Group, 5651CA Eindhoven, The Netherlands (e-mail: frank.achten@prysmiangroup.com).

Ali Mefleh is with the KPN, 2500GA The Hague, The Netherlands (e-mail: ali.mefleh@kpn.com).

Cristian Antonelli is with the University of L'Aquila and CNIT, 67100 L'Aquila, Italy (e-mail: cristian.antonelli@univaq.it).

Chigo Okonkwo is with the High Capacity Optical Transmission Laboratory, Electro-Optical Communications Group, Eindhoven University of Technology, 5600 MB Eindhoven, The Netherlands (e-mail: c.m.okonkwo@tue.nl).

Georg Rademacher was with the Photonic Network System Laboratory, National Institute of Information and Communications Technology, Koganei 184-8795, Japan. He is now with the Institute of Electrical and Optical Communications, University of Stuttgart, 70174 Stuttgart, Germany (e-mail: georg.rademacher@int.uni-stuttgart.de).

Color versions of one or more figures in this article are available at <https://doi.org/10.1109/JLT.2023.3316832>.

Digital Object Identifier 10.1109/JLT.2023.3316832

current demonstrations have been limited to mostly short-distance high-mode count or long-distance low-mode count transmission. In this work, we transmit 15 modes \times 184 wavelength channels \times 24.5 GBd PDM-16-QAM signals, spanning the full C-band, over 1001 km of 15-mode multi-mode fiber. The resulting net data rate of 273.6 Tb/s is the highest reported data rate in long-distance multi-mode fiber transmission and results in a record capacity-distance product of 273.9 Pb/s-km for multi-mode transmission. This was achieved by using mode multiplexers with low mode-dependent loss (MDL) and insertion loss, as well as a 15-mode fiber optimized for a low differential mode delay (DMD) transmission regime.

Index Terms—Space-division multiplexing, optical transmission, multi-mode fiber, long-haul transmission.

I. INTRODUCTION

OVER the past years, the potential of space-division multiplexing (SDM) [1] to increase optical fiber transmission data rates by modulating independent data signals on independent spatial paths has been shown, allowing to overcome the potential capacity limits of single-mode fiber-based networks [2]. In multi-core fibers (MCFs), multiple cores inside a single cladding are used, and for multi-mode fibers (MMFs), multiple spatial modes inside a single core are used as independent spatial paths, while the hybrid combination of MCF and MMF has potentially the highest amount of spatial paths inside a single fiber. Recently, however, SDM fibers which maintain the current standard cladding diameter of 125 μ m have gained interest, as these fibers can benefit from current manufacturing, cabling, and installation techniques, already optimized for this cladding diameter. Next to this, 125 μ m cladding diameter fibers are reported to have higher reliability and production yield in comparison to larger cladding diameter fibers [3]. Whilst maintaining the 125 μ m cladding diameter, the maximum number of spatial paths in MCFs is limited to about four paths for uncoupled [4] MCF in the C-band and 19 paths is the maximum reported for coupled MCF [5]. As modes inside a MMF spatially overlap, it is apparent that those fibers have the potential for supporting high

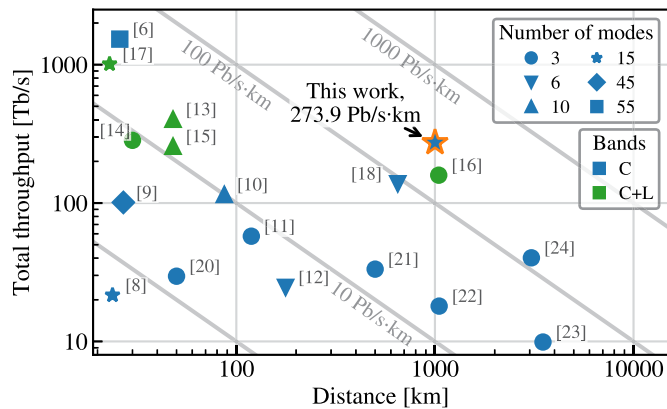


Fig. 1. Overview of recent multi-mode transmission experiments, indicating that up to now, long-distance multi-mode transmission was limited to mostly 3- and 6-mode transmission. Diagonal lines represent constant capacity-distance products.

numbers of spatial paths. However, mode-dependent loss (MDL) and delay spread increase for a larger number of modes and are typically higher compared to coupled MCFs, and thus need to be managed carefully. Transmission over a 55-mode MMF has recently been shown [6], and MMFs potentially supporting an even higher number of modes can be manufactured by slightly increasing the fiber core size.

Previous transmission experiments employing 125 μm cladding diameter MMFs have been summarized in Fig. 1. Short-distance transmission using MMFs guiding up to 55 modes has been demonstrated [7], [8], [9], [10], [11], [12], [13], [14], [15], [16], [17], with 55 mode transmission limited to 25.9 km with a data rate of 1.53 Pb/s [6]. Long-distance transmission, on the other hand, used to be mostly limited to 3 or 6-mode transmission [16], [18], [19], [20], [21], [22], [23], [24], as can be seen in Fig. 1. Notable is also the first 10-mode transmission over 1300 km from [25] presented at the same time as our original work [26], but this is not included in Fig. 1 as the total throughput was not measured.

In addition to increasing the number of transmitted modes, the total per-fiber throughput can also be increased by transmitting wavelength-division multiplexed (WDM) signals outside the conventional C-band, as is for example shown in [16]. There, 3-mode transmission resulted in a data rate of 159 Tb/s after transmission over 1045 km, using WDM signals in both C+L bands. The usage of signals in different spectra outside the C-band comes at the cost of more complex amplification schemes, as it requires per-band amplification. This complicates the already challenging task of designing and fabricating multi-mode amplifiers for in-line amplification.

For long-distance multi-mode transmission, MDL and differential mode delay (DMD) are important performance-limiting effects. MDL fundamentally limits the overall system performance due to unequal attenuation of the spatial modes in inline components and the fiber. DMD increases the impulse response duration proportional to the transmission distance, as the different spatial modes propagate with different speeds through the fiber. This does not fundamentally limit the performance of the transmission, but when the impulse response duration becomes too long, the memory length of the multiple-input multiple-output (MIMO) digital filter becomes impractical [27]. Hence, low

MDL and a short impulse response duration are key for practical SDM systems.

In this work, we extend our previous work published in [26] and demonstrate long-haul and high-capacity data transmission over a standard 125 μm cladding diameter 15-mode MMF. The transmission link is DMD uncompensated, and we employ a cyclic mode group permutation technique as proposed in [19] in order to limit the total delay spread and thus impulse response duration of the transmission system. The spatial mode (de)multiplexers we use have low MDL (< 3 dB) and have a low insertion loss (< 4.5 dB) [28]. The 15-mode fiber used for transmission has an inherently low DMD (< 100 ps/km) [29], limiting the delay spread of the system. The fiber used in this experiment is of the same type as the deployed 15-mode fiber in the testbed in the city of L'Aquila, Italy, and has been previously characterized and used for field-deployed transmission [30], [31]. Compared to our previous publication [26], we include more details about the 15-mode fiber, characterize the mode-multiplexer, analyze MDL and the related performance penalty resulting from MDL. Combination of the low-MDL multiplexers and optimized multi-mode fiber results in the transmission of 15 modes \times 184 wavelength channels \times 24.5 GBd PDM-16-QAM C-band signals over 1001 km of 15-mode MMF using a recirculating loop setup with a span length of 58.9 km. The resulting total data rate is 312.6 Tb/s based on generalized mutual information (GMI) calculation and a data rate of 273.6 Tb/s after decoding is measured, which is the highest reported data rate for long-haul transmission in MMF and results in a record capacity-distance product of 273.9 Pb/s-km for MMF.

The remainder of this article is structured as follows; Sections II and III describe the transmission fiber and mode multiplexers in more detail, Section IV presents the experimental setup, in Section V the transmission channel is characterized while Section VI presents the transmission results. Finally, the article is concluded in Section VII.

II. 15-MODE MULTI-MODE FIBER

The MMF [29] used for transmission was optimized to guide 15 spatial modes with a low DMD using the process described in [32]. As the optimized trench-assisted graded-index profile was similar to that of a standard 50 μm core diameter MMF, appropriately scaled trench-assisted bend-insensitive multi-mode preforms were used to fabricate the 15-mode fiber with a core diameter of 28 μm . The normalized frequency V was set slightly below 11.8 at 1550 nm to ensure that only the first five mode groups were guided and it was confirmed by measurements that undesired higher-order modes were cut-off for C-band wavelengths and above. Also, the graded-index core exponent (α) was optimized to ensure low DMD at 1550 nm. This resulted in the refractive index profile shown in Fig. 2, where the spatial modes are depicted. Being able to use standard multi-mode manufacturing processes with tight tolerances for fabrication resulted in low DMD values of 100 ps/km at 1550 nm and the attenuation per mode varied between 0.21 dB/km and 0.24 dB/km for the 15 spatial modes at 1550 nm [17, Fig. 3d]. Mode-groups 1 to 4 all had an attenuation below 0.22 dB/km, while the attenuation of the fifth mode-group was 0.24 dB/km, originating from an increase in micro-bending sensitivity due to lower effective indexes in this mode group [33]. Attenuation was measured by exciting each input mode of a 23 km long piece of fiber using a mode-multiplexer

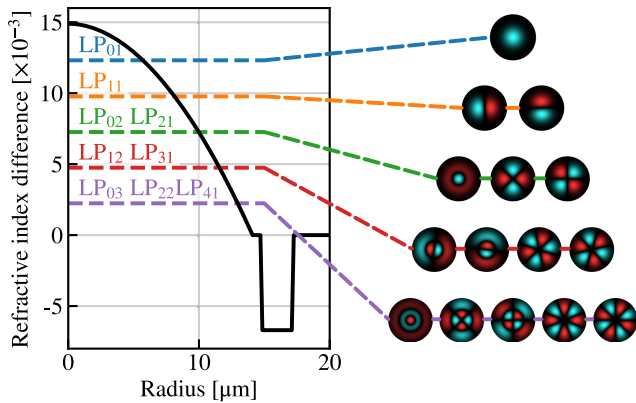


Fig. 2. Refractive index profile of the 15-mode MMF and the corresponding spatial modes. Modes which have similar effective refractive indices are grouped into mode groups.

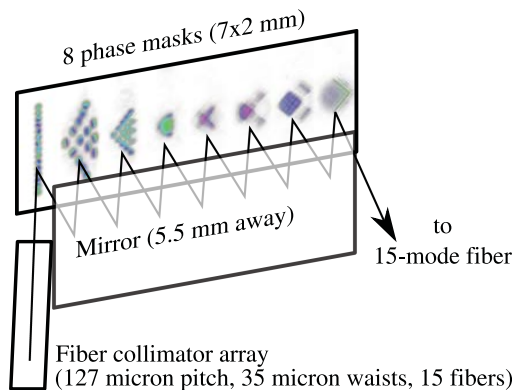


Fig. 3. Schematic of working principle of MPLC based mode multiplexer. The 15 single mode beams from the fiber collimator array are converted into the 15 fiber modes by reflection between phase masks and a mirror.

and measuring the total power at the output. The 58.9 km long span of MMF used in the experiment consisted of 10 spools of fiber with lengths varying from 4.4 km to 15.2 km, which were fusion spliced together. Splice points could potentially introduce additional MDL when fibers are misaligned. However, using commercially available fusion splicers, it is possible to align both fibers sufficiently accurately to obtain a negligible MDL impact [34].

III. MODE MULTIPLEXERS

Mode (de)multiplexers based on multi-plane light converter (MPLC) [28], [35] technology were used. Fig. 3 shows the working principle of MPLC based mode multiplexers. An array of 15 single-mode spots is created by a fiber collimator array. The output beams of this collimator array are converted to the 15 fiber modes by bouncing between phase masks and a mirror. Finally, the output of the multiplexer is coupled into the 15-mode MMF. The phase masks are designed using an *inverse design* technique as described in [36] and establish a mode-selective relation between the 15 single-mode inputs and the 15 fiber modes.

A single multiplexer has been characterized [28] using a digital holography (DH) [37], [38] based characterization setup, of which the results are presented in Fig. 4. DH allows characterization of SDM devices at a component level. As can be seen, the

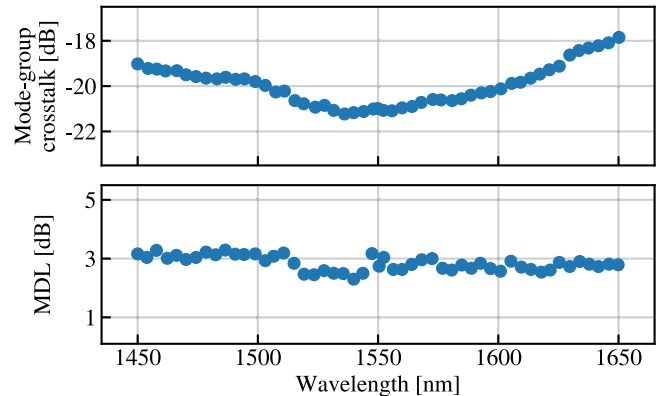


Fig. 4. Mode group crosstalk and MDL of the MPLC based mode multiplexer, after [28].

multiplexers have low mode-group crosstalk and low MDL over a broad wavelength range, allowing transmission beyond the conventional C-band window. Here, mode-group crosstalk is defined as the ratio between the power in the intended mode-groups and the other mode-groups and gives an indication of the mode-group selectivity of the multiplexer. As crosstalk between modes is removed in the MIMO equalizer at the receiver, crosstalk itself is not limiting the transmission performance. However, for the mode-group permutation scheme described in the next section, good mode-selectivity is required to allow permutation between modes. It should also be noted that the measured minimum MDL of 3 dB appeared to be a noise floor of the measurement setup (resulting from uncompensated losses in pigtailed), rather than originating from the device itself. Furthermore, an insertion loss in the order of 4.5 dB was measured around 1550 nm.

IV. TRANSMISSION SETUP

The experimental transmission setup to demonstrate 15-mode transmission is presented in Fig. 5. The transmitter comprised a 3-channel test band and a noise loading stage filling the C-band to emulate full WDM transmission [39]. The 25 GHz spaced 3-channel test band was generated by modulating tones produced by 3 external cavity lasers (ECLs) with a linewidth below 10 kHz using two dual-polarization IQ-modulators (DP-IQMs). The center test channel was modulated using a dedicated DP-IQM, while the two neighbouring tones were combined and modulated using a second DP-IQM. Both DP-IQMs were driven by the same 4-channel 65 GS/s arbitrary-waveform generator (AWG) that was programmed to generate 24.5 GBd 16-ary quadrature amplitude modulation (QAM) signals with a pattern length of $2^{17} - 1$ symbols, pulse shaped with a 1% root-raised-cosine (RRC) filter. The C-band filling noise loading band was produced by generating amplified spontaneous emission (ASE) using two erbiumdoped fiber amplifiers (EDFAs), where an optical processor (OP) was used to flatten the resulting spectrum. The OP was also used to carve a notch in the noise loading band around the frequencies of the test band, allowing the combination of the test band and noise loading band using a power combiner.

The resulting signal was passed through an acousto-optic modulator (AOM), which served as a load switch for the recirculating loop. Next, the signal was split and delayed to generate 15 tributaries with a relative delay of 150 ns. These tributaries

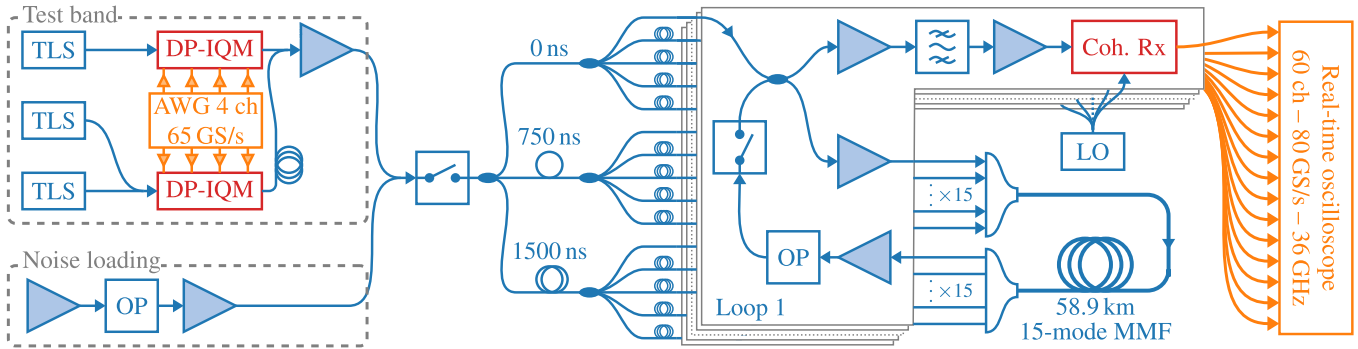


Fig. 5. Experimental transmission setup. A 3 channel test band is combined with a C-band spanning noise loading stage to emulate full C-band transmission. The resulting signal is split and delayed to generate 15 tributaries with a relative delay of 150 ns which enter the recirculating loop. The outputs of the recirculating loop are detected by a 60 channel oscilloscope.

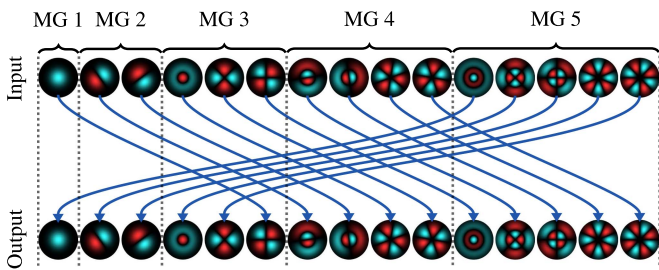


Fig. 6. Visual representation of the employed mode group permutation scheme. The single mode outputs of the mode de-multiplexer at the output of the MMF are connected in such a way that all modes in a mode group are converted to a mode from a different mode group in order to reduce delay spread.

were fed into 15 parallel path-length aligned recirculating loops. The loops consisted of EDFAs to compensate for attenuation due to the fiber and loop components, as well as an OP for flattening of the spectrum and an AOM that acted as a loop switch. The relative delay between the 15 parallel loops was matched to be within 1 cm (50 ps), which is considerably lower than the DMD of the fiber. The single mode outputs of the 15 loops were amplified to 21.5 dBm and multiplexed using the mode multiplexer described in Section III. The resulting 15-mode signal was transmitted over a 58.9 km long span of 15-mode fiber, see Section II, and demultiplexed using a second MPLC.

To mitigate the accumulation of DMD in MMFs, strong mode coupling can be intentionally introduced. Indeed, in the regime of strong mode mixing, the DMD accumulates with the square root of distance compared to linearly in the regime of weak mode coupling [40], [41]. Operation in the strongly-coupled regime can be forced by inserting mode scramblers in the transmission link. This technique has been demonstrated in [19], [25], [42] based on mode-permutations in mode (de)multiplexer pairs up to 10-mode transmission. A similar mode group permutation technique was introduced into the 15-mode transmission experiment by connecting the 15 single mode outputs of the mode demultiplexer to the inputs of the 15 recirculating loops, see Fig. 6. The connections were made in such a way that the mode groups were cyclically permuted, making sure that modes are forced into a different mode group. By permuting modes between mode groups, the propagation time per mode is equalized, as the propagation speed is mostly constant within a single mode group. Similarly, the permutation

technique might be beneficial for MDL, as MDL grows with the square root of distance in the strongly-coupled regime, compared to linear growth in weakly-coupled systems.

In order to receive the 15-mode signal, the outputs of the 15 parallel loops were amplified using EDFAs and the channel under test (CUT) was filtered using tunable filters and amplified again before being received by 15 coherent receivers (CRXs) sharing the same local oscillator (LO) that had a linewidth below 60 kHz. The electrical signals from the CRXs were digitized by a 60-channel, 80 GS/s, real-time oscilloscope with a bandwidth of 36 GHz. The resulting samples were processed by an offline digital signal processing (DSP) chain that consisted mostly of a 30×30 time-domain MIMO equalizer with 1801 half-symbol-duration-spaced taps that were initialized in a data-aided mode before switching to a decision-directed least means squares (LMS) mode for signal performance estimation. Inside the equalizer loop, a decision-directed phase recovery algorithm [43] was running.

V. TRANSMISSION CHANNEL CHARACTERIZATION

In Fig. 7 the coupling matrices of the transmission channel are shown for different transmission distances. The coupling matrices are obtained from the taps of the 30×30 MIMO equalizer, which are averaged over both polarizations to obtain a 15×15 matrix. As can be seen from Fig. 7(a), before transmission over the MMF, the coupling matrix resembles a diagonal matrix, indicating no coupling between the modes. After one recirculation, Fig. 7(b), the mode groups are cyclically permuted and hence the coupling matrix does no longer resemble a diagonal matrix. Additionally, it can be observed how modes couple mostly within the same mode group after one recirculation, while after two recirculations, Fig. 7(c), strong coupling between all the modes can already be observed, as induced by the cyclic mode permutation scheme. Fig. 7(d) shows the coupling matrix after 17 circulations, equivalent to transmission over 1001 km, and shows that the modes are fully mixed.

The intensity impulse response (IIR) for a channel at 1533.9nm for different transmission distances is shown in Fig. 8, showing that the IIR gradually evolves to a Gaussian-shaped response for longer distances. Also, an increase in the noise floor of the equalizer taps can be observed for longer transmission distances. This might be due to additional noise at these distances, preventing the equalizer taps from properly converging. Based on the measured IIRs, we calculate the intensity impulse

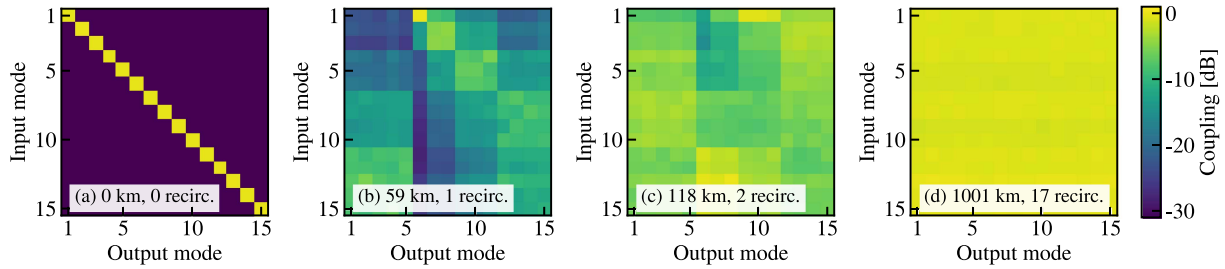


Fig. 7. Normalized coupling matrices obtained from the MIMO equalizer for different transmission distances. Comparing (a) and (b) clearly shows the effect of mode permutation; the coupling matrix is no longer a diagonal matrix after the first recirculation.

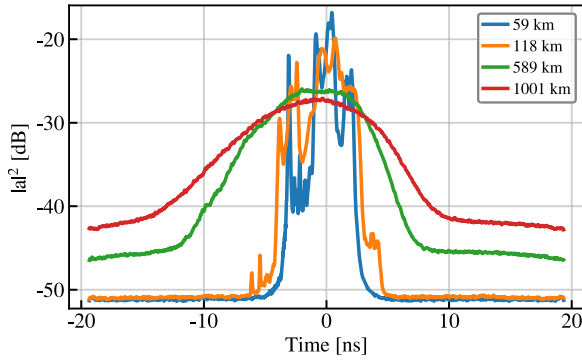


Fig. 8. Intensity impulse response for after different transmission distances measured at 1533.9 nm. For longer transmission distances, the response becomes Gaussian-shaped.

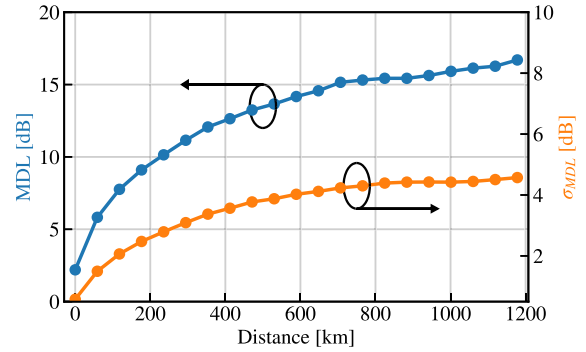


Fig. 11. MDL for a channel at 1545.7 nm obtained from the taps of the MIMO equalizer versus transmission distance. Both the min-max MDL and the standard deviation MDL are given.

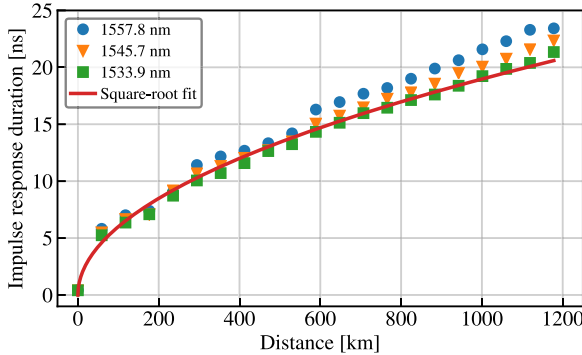


Fig. 9. Impulse response duration versus transmission distance. The square-root relation indicates operation in the strong-coupling regime.

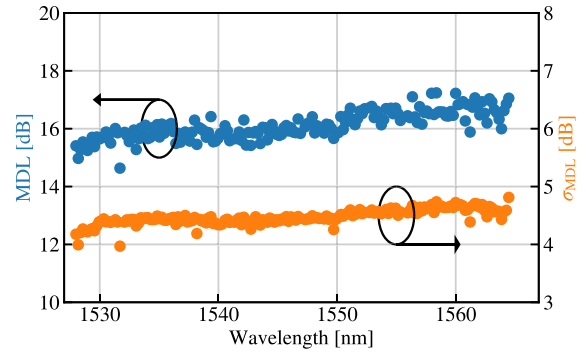


Fig. 12. MDL obtained from the taps of the MIMO equalizer after transmission over 1001 km. Both the min-max MDL and the standard deviation MDL are given.

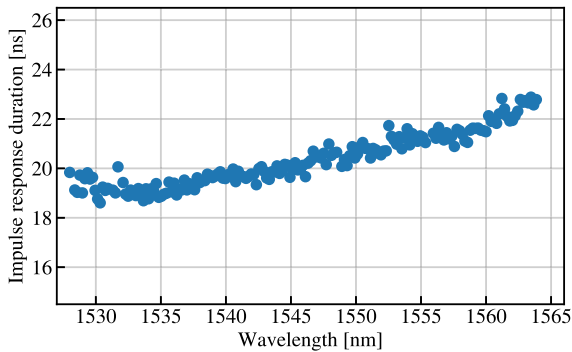


Fig. 10. Impulse response duration versus wavelength after transmission over 1001 km, the wavelength dependence of the DMD results in 4 ns variation across the C-band.

response duration. We define this duration arbitrarily as the time that covers 98% of the energy in the intensity impulse response. The IIR duration versus transmission distance is measured for three different wavelength channels and shown in Fig. 9, together with a square-root fit. From there we see a similar relation for all three wavelengths, with a minor variation in the total IIR duration due to the wavelength dependence of the DMD. Also, a square-root relation between the IIR duration and transmission distance can be observed, suggesting transmission in the strong-coupling regime. The IIR duration for all wavelength channels after transmission over 1001 km is shown in Fig. 10. The wavelength dependence of the DMD is a fiber property, as also seen in [17], and results in a variation of the IIR duration of 4 ns across the full C-band.

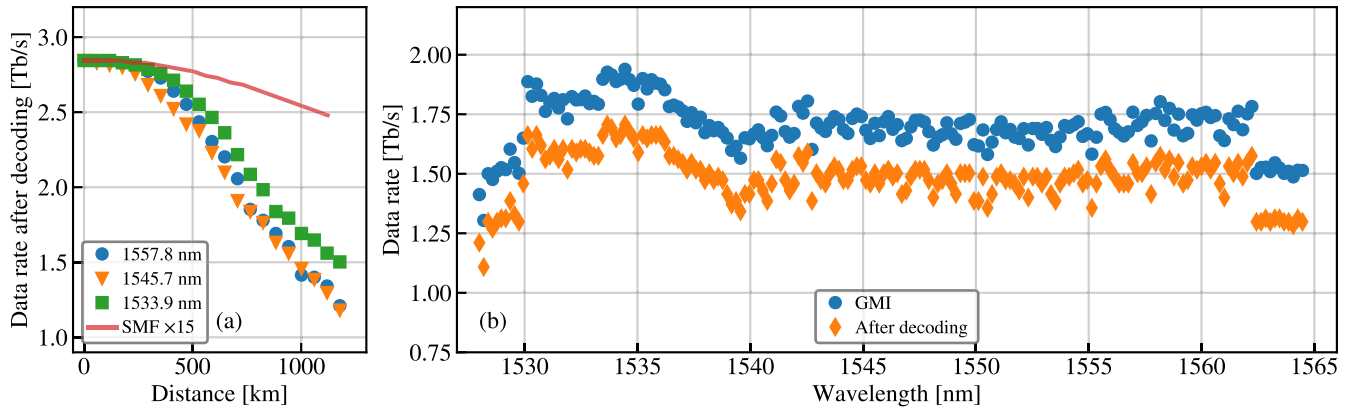


Fig. 13. (a) Shows the data rate after decoding versus transmission distance and (b) shows the data rate based on GMI and after decoding for all measured wavelength channels.

Furthermore, we investigate the MDL in the transmission experiment. To this end, we apply a singular-value decomposition on the transmission channel matrix obtained from the taps of the MIMO equalizer to obtain the related eigenvalues. These are averaged over the channel bandwidth and the MDL is evaluated by calculating the difference between the minimum and maximum eigenvalues, or by taking the standard deviation of the eigenvalues [44]. Fig. 11 shows the MDL versus transmission distance, showing its increase with distance. In Fig. 12 the MDL is plotted after transmission over 1001 km for all measured wavelength channels. The average min-max MDL was 16 dB and σ_{MDL} of 4.5 dB, furthermore the MDL was reasonably flat over all wavelengths.

VI. TRANSMISSION RESULTS

Fig. 13 summarizes the results of the transmission demonstration. Net data rates were calculated based on GMI and using a decoding scheme which is described in more detail in [17]. This scheme applied codes from the DVB-S2 [45] standard in combination with code-rate puncturing to achieve a bit error rate (BER) below 5×10^{-5} with an additional hard-decision outer forward error correction (FEC) code with 1% overhead to eliminate remaining bit errors [46]. The data rates of the transmission demonstration are shown as a function of the transmission distance for 3 wavelength channels across the C-band in Fig. 13(a), and shows there is a simple trade-off between total data rate and transmission distance. For comparison between the 15-mode fiber system and a 15-parallel single-mode fiber transmission system, we also measured the throughput of single-mode fiber with a similar length that was placed inside the recirculating loop. An attenuator of 10 dB was placed in the loop to emulate the losses of the mode (de)multiplexer pair. Fig. 13(a) shows the decoded throughput measured using this system, multiplied by 15 to indicate the combined throughput of 15 of those systems. The data rate of the 15-mode systems decays faster compared to the single-mode system due to MDL, resulting in a penalty compared to 15 parallel systems. Fig. 13(b) shows the data rate for all measured wavelength channels based on both GMI and data rate after decoding, after transmission over 1001 km. Per channel data rate after decoding varied between 1.1 Tb/s and 1.7 Tb/s. The difference in performance across the wavelength channels is believed to arise from the EDFA gain profile of the loop amplifiers and component limitations

reducing the performance of the upper C-band channels and not from the 15-mode fiber itself.

The data rates per channel were on average 1.70 Tb/s based on GMI estimation and 1.47 Tb/s after decoding, resulting in an overall data rate of 312.6 Tb/s based on GMI and 273.6 Tb/s after decoding, which is the highest reported data rate for long-distance (> 60 km) MMF transmission. Based on the decoded data rates, the capacity-distance product is 273.9 Pb/s-km, which is the highest reported in a MMF transmission system. These results indicate the strong potential of MMFs for long-haul, high-capacity links.

VII. CONCLUSION

We have demonstrated long-haul, high-capacity transmission over 1001 km of 15-mode differential mode delay (DMD) uncompensated fiber. We used mode multiplexers with low insertion loss and mode-dependent loss (MDL), a 15-mode fiber with low DMD and a mode group permutation technique to reduce the total delay spread due to DMD. We transmitted $15 \times 184 \times 24.5$ GBd PDM-16-QAM, spanning more than 35 nm across the C-band, resulting in a decoded net data rate of 273.6 Tb/s, the highest reported data rate in long-distance multi-mode fiber (MMF) transmission, and resulting in a record capacity-distance product for MMFs of 273.9 Pb/s-km. This highlights the strong potential of MMF transmission systems for future long-haul, high-capacity links. Furthermore, the wideband operation of the used mode multiplexers allows for transmission outside the C-band, allowing for a further increase of throughput by extending transmission into S- and L-band.

REFERENCES

- [1] B. J. Puttnam, G. Rademacher, and R. S. Luís, "Space-division multiplexing for optical fiber communications," *Optica*, vol. 8, no. 9, 2021, pp. 1186–1203.
- [2] P. J. Winzer and D. T. Neilson, "From scaling disparities to integrated parallelism: A Decathlon for a decade," *J. Lightw. Technol.*, vol. 35, no. 5, pp. 1099–1115, Mar. 2017.
- [3] T. Matsui, P. L. Pondillo, and K. Nakajima, "Weakly coupled multicore fiber technology, deployment and systems," *Proc. IEEE*, vol. 110, no. 11, pp. 1772–1785, Nov. 2022.
- [4] T. Matsui, P. L. Pondillo, and K. Nakajima, "Weakly coupled multicore fiber technology, deployment, and systems," *Proc. IEEE*, vol. 110, no. 11, pp. 1772–1785, Nov. 2022.

- [5] G. Rademacher et al., "Randomly coupled 19-core multi-core fiber with standard cladding diameter," in *Proc. IEEE Opt. Fiber Commun. Conf. Exhib.*, 2023, pp. 1–3.
- [6] G. Rademacher et al., "1.53 peta-bit/s C-band transmission in a 55-Mode fiber," in *Proc. IEEE Eur. Conf. Opt. Commun.*, 2022, pp. 1–4. [Online]. Available: <https://opg.optica.org/abstract.cfm?URI=ECEOC-2022-Th3C.3>
- [7] S. Beppu et al., "402.7-Tb/s MDM-WDM transmission over weakly coupled 10-Mode fiber using rate-adaptive PS-16QAM signals," *J. Lightw. Technol.*, vol. 38, no. 10, pp. 2835–2841, May 2020.
- [8] N. K. Fontaine et al., "3030 MIMO Transmission Over 15 Spatial Modes," in *Proc. IEEE Opt. Fiber Commun. Conf.*, 2015, pp. 1–3.
- [9] R. Ryf et al., "High-spectral-efficiency mode-multiplexed transmission over graded-index multimode fiber," in *Proc. IEEE Eur. Conf. Opt. Commun.*, 2018, pp. 1–3.
- [10] R. Ryf et al., "10-mode mode-multiplexed transmission over 125-km single-span multimode fiber," in *Proc. IEEE Eur. Conf. Opt. Commun.*, 2015, pp. 1–3.
- [11] V. Sleiffer et al., "73.7 Tb/s ($96 \times 3 \times 256$ -Gb/s) mode-division-multiplexed DP-16QAM transmission with inline MM-EDFA," *Opt. Exp.*, vol. 20, no. 26, pp. B428–B438, Dec. 2012. [Online]. Available: <https://opg.optica.org/oe/abstract.cfm?URI=oe-20-26-B428>
- [12] R. Ryf et al., "32-bit/s/hz spectral efficiency WDM transmission over 177-km few-mode fiber," in *Proc. IEEE Opt. Fiber Commun. Conf. Expo. Nat. Fiber Optic Engineers Conf.*, 2013, pp. 1–3.
- [13] D. Soma et al., "402.7-Tb/s weakly-coupled 10-mode-multiplexed transmission using rate-adaptive PS PDM-16QAM WDM signals," in *Proc. IEEE 45th Eur. Conf. Opt. Commun.*, 2019, pp. 1–4.
- [14] G. Rademacher et al., "93.34 Tbit/s/mode (280 Tbit/s) transmission in a 3-mode graded-index few-mode fiber," in *Proc. IEEE Opt. Fiber Commun. Conf. Expo.*, 2018, pp. 1–3.
- [15] D. Soma, S. Beppu, Y. Wakayama, Y. Kawaguchi, K. Igarashi, and T. Tsuritani, "257-Tbit/s partial MIMO-based 10-mode C+ L-band WDM transmission over 48-km FMF," in *Proc. IEEE Eur. Conf. Opt. Commun.*, 2017, pp. 1–3.
- [16] G. Rademacher et al., "159 Tbit/s C + L band transmission over 1045 km 3-Mode graded-index few-mode fiber," in *Proc. IEEE Opt. Fiber Commun. Conf.*, 2018, pp. 1–3. [Online]. Available: <https://opg.optica.org/abstract.cfm?URI=OFC-2018-Th4C.4>
- [17] G. Rademacher et al., "Peta-bit-per-second optical communications system using a standard cladding diameter 15-mode fiber," *Nature Commun.*, vol. 12, no. 1, Jul. 2021, Art. no. 4238, doi: [10.1038/s41467-021-24409-w](https://doi.org/10.1038/s41467-021-24409-w).
- [18] J. van Weerdenburg et al., "138-Tb/s mode- and wavelength-multiplexed transmission over six-mode graded-index fiber," *J. Lightw. Technol.*, vol. 36, no. 6, pp. 1369–1374, Mar. 2018.
- [19] K. Shibahara, T. Mizuno, H. Ono, K. Nakajima, and Y. Miyamoto, "Long-haul DMD-Unmanaged 6-Mode-Multiplexed transmission employing cyclic mode-group permutation," in *Proc. IEEE Opt. Fiber Commun. Conf. Exhib.*, 2020, pp. 1–3.
- [20] E. Ip et al., "88×3×112-Gb/s WDM transmission over 50 km of three-mode fiber with inline few-mode fiber amplifier," in *Proc. IEEE 37th Eur. Conf. Exhib. Opt. Commun.*, 2011, pp. 1–3.
- [21] E. Ip et al., "146 × 6 × 19-Gbaud wavelength-and mode-division multiplexed transmission over 10 × 50-km spans of few-mode fiber with a gain-equalized few-mode EDFA," *J. Lightw. Technol.*, vol. 32, no. 4, pp. 790–797, Feb. 2014.
- [22] R. Ryf et al., "Distributed Raman amplification based transmission over 1050-km few-mode fiber," in *Proc. IEEE Eur. Conf. Opt. Commun.*, 2015, pp. 1–3.
- [23] G. Rademacher et al., "3500-km mode-multiplexed transmission through a three-mode graded-index few-mode fiber link," in *Proc. IEEE Eur. Conf. Opt. Commun.*, 2017, pp. 1–3.
- [24] K. Shibahara et al., "Full C-band 3060-km DMD-unmanaged 3-mode transmission with 40.2-Tb/s capacity using cyclic mode permutation," *J. Lightw. Technol.*, vol. 38, no. 2, pp. 514–521, Jan. 2020.
- [25] K. Shibahara, M. Hoshi, and Y. Miyamoto, "10-Spatial-Mode 1300-Km Transmission Over 6-LP Graded Index Few-Mode Fiber With 36-Ns Modal Dispersion," in *Proc. IEEE Opt. Fiber Commun. Conf.*, 2023, pp. 1–3.
- [26] M. van den Hout et al., "273.6 Tb/s transmission over 1001 km of 15-Mode fiber using 16-QAM C-band signals," in *Proc. IEEE Opt. Fiber Commun. Conf. Exhib.*, 2023, pp. 1–3.
- [27] B. Inan et al., "DSP complexity of mode-division multiplexed receivers," *Opt. Exp.*, vol. 20, no. 10, pp. 10859–10869, May 2012. [Online]. Available: <https://opg.optica.org/oe/abstract.cfm?URI=oe-20-10-10859>
- [28] N. K. Fontaine et al., "Broadband 15-mode multiplexers based on multi-plane light conversion with 8 planes in unwrapped phase space," in *Proc. IEEE Eur. Conf. Opt. Commun.*, 2022, pp. 1–4.
- [29] P. Sillard et al., "Low-differential-mode-group-delay 9-LP-Mode fiber," *J. Lightw. Technol.*, vol. 34, no. 2, pp. 425–430, Jan. 2016.
- [30] G. Rademacher et al., "Characterization of the first field-deployed 15-mode fiber cable for high density space-division multiplexing," in *Proc. Eur. Conf. Opt. Commun.*, 2022, pp. 1–4.
- [31] L. Dallachiesa et al., "Mode-group-division multiplexing over a deployed 15-mode-fiber cable," in *Proc. IEEE Opt. Fiber Commun. Conf. Exhib.*, 2023, pp. 1–3.
- [32] P. Sillard, M. Bigot-Astruc, and D. Molin, "Few-mode fibers for mode-division-multiplexed systems," *J. Lightw. Technol.*, vol. 32, no. 16, pp. 2824–2829, Aug. 2014.
- [33] P. Sillard et al., "Micro-bend-resistant low-differential-mode-group-delay few-mode fibers," *J. Lightw. Technol.*, vol. 35, no. 4, pp. 734–740, Feb. 2017. [Online]. Available: <https://opg.optica.org/jlt/abstract.cfm?URI=jlt-35-4-734>
- [34] G. Rademacher et al., "Experimental investigation of coupling offset tolerances in a space-division multiplexed 15-mode fiber transmission system," in *Proc. IEEE Eur. Conf. Opt. Commun.*, 2022, pp. 1–4.
- [35] G. Labroille, B. Denolle, P. Jian, J.-F. Morizur, P. Genevaux, and N. Treps, "Efficient and mode selective spatial mode multiplexer based on multi-plane light conversion," in *Proc. IEEE Photon. Conf.*, 2014, pp. 518–519.
- [36] N. K. Fontaine, R. Ryf, H. Chen, D. T. Neilson, K. Kim, and J. Carpenter, "Laguerre-Gaussian mode sorter," *Nature Commun.*, vol. 10, Apr. 2019, Art. no. 1865.
- [37] M. Mazur et al., "Characterization of long multi-mode fiber links using digital holography," in *Proc. IEEE Opt. Fiber Commun. Conf.*, 2019, pp. 1–3.
- [38] S. P. van der Heide et al., "Exploiting angular multiplexing for polarization-diversity in Off-Axis digital holography," in *Proc. IEEE Eur. Conf. Opt. Commun.*, 2020, pp. 1–4.
- [39] D. J. Elson et al., "Investigation of bandwidth loading in optical fibre transmission using amplified spontaneous emission noise," *Opt. Exp.*, vol. 25, no. 16, pp. 19529–19537, Aug. 2017. [Online]. Available: <https://opg.optica.org/oe/abstract.cfm?URI=oe-25-16-19529>
- [40] C. Antonelli, A. Mecozzi, M. Shtaf, and P. J. Winzer, "Stokes-space analysis of modal dispersion in fibers with multiple mode transmission," *Opt. Exp.*, vol. 20, no. 11, pp. 11718–11733, 2012.
- [41] S. O. Arik, K.-P. Ho, and J. M. Kahn, "Group delay management and multiinput multioutput signal processing in mode-division multiplexing systems," *J. Lightw. Technol.*, vol. 34, no. 11, pp. 2867–2880, Jun. 2016.
- [42] K. Shibahara et al., "DMD-Unmanaged long-haul SDM transmission over 2500-km 12-Core 3-Mode MC-FMF and 6300-km 3-Mode FMF employing intermodal interference canceling technique," *J. Lightw. Technol.*, vol. 37, no. 1, pp. 138–147, Jan. 2019.
- [43] T. Pfau, S. Hoffmann, and R. Noe, "Hardware-efficient coherent digital receiver concept with feedforward carrier recovery for M-QAM constellations," *J. Lightw. Technol.*, vol. 27, no. 8, pp. 989–999, Apr. 2009.
- [44] R. S. B. Ospina et al., "Mode-dependent loss and gain estimation in SDM transmission based on MMSE equalizers," *J. Lightw. Technol.*, vol. 39, no. 7, pp. 1968–1975, Apr. 2021.
- [45] *Digital Video Broadcasting (DVB); Second Generation Framing Structure, Channel Coding and Modulation Systems for Broadcasting, Interactive Services, News Gathering and other Broadband Satellite Applications; Part 1: DVB-S2*. ETSI Standard ETSI EN 302 307-1, 2014.
- [46] D. S. Millar et al., "Design of a 1 Tb/s superchannel coherent receiver," *J. Lightw. Technol.*, vol. 34, no. 6, pp. 1453–1463, Mar. 2016.